EFFECTS OF ZINC OXIDE STRUCTURES ON VARIOUS PROPERTIES OF ZINC OXIDE EUGENOL USED IN DENTISTRY

SITI KHADIJAH BINTI MOHD BAKHORI

UNIVERSITI SAINS MALAYSIA

2018

EFFECTS OF ZINC OXIDE STRUCTURES ON VARIOUS PROPERTIES OF ZINC OXIDE EUGENOL USED IN DENTISTRY

by

SITI KHADIJAH BINTI MOHD BAKHORI

Thesis submitted in fulfillment of the requirements
for the degree of
Doctor of Philosophy

August 2018

ACKNOWLEDGEMENT

In the name of Allah, the Most Gracious, Most Merciful. Foremost of all, I thank the Almighty Allah for giving me inspiration, patience and good health which enable me to complete this study and dissertation.

I owe the greatest gratitude to my main supervisor, Assoc. Prof. Dr. Shahrom Mahmud for his guidance and supervision as well as patience throughout the course of my research. I admire his attitude in doing research that involved multi-disciplinary niche area. I also want to thank my co- supervisors, Prof. Sam'an Malik Masudi (expert in dental material studies), Assoc. Prof. Dr. Dasmawati Mohamad (expert in microbiology studies) and Assoc. Prof. Dr. Md Azman Seeni Mohamed (expert in toxicology studies) for their assistance and many invaluable suggestions and support carrying antibacterial and cytotoxicity studies. Their good research laboratory and expertise had convenience me in completing all the biology related experiments.

I wish to express my appreciation to all my colleagues and research members in NOR lab (School of Physics), Craniofacial Lab (School of Dental Science, USM), Microbiology and Parasitology Lab (School of Medicine Science USM), Integrative Medicine Cluster and Advance Diagnostic Lab (IPPT), especially Dr. Ling Chuo Ann, Dr. Amna Sirelkhatim, Mrs. Rosliza Abd Rahman, Mrs. Siti Nazmin Saifuddin, Mr. Zulkifli Ismail for their expertise, technical assistance and contribution to my work.

Finally, I extend my sincere thanks to my family for their full support and encouragement. A special thanks to my parents, husband and children for supporting me from beginning until the end.

TABLE OF CONTENTS

Acknowledgement		ii
Table of contents		iii
List of tables		ix
List of figures		x
List of abbreviations		xvii
List of symbols		xx
Abstrak		xxi
Abstract		xxiii

CHAPTER 1 - INTRODUCTION

1.1	Introduction	1
1.2	ZnO eugenol	2
1.3	Oral bacteria	5
1.4	Background of the study	6
1.5	Problem statement and Novelty of the studies	7
1.6	Objectives of the study	8
1.7	Scope of the study	9
1.8	Overview of the study	10

CHAPTER 2 - LITERATURE REVIEW

2.1	Introduction	12
2.2	Application of ZnO	13
2.3	Properties of ZnO	13
2.4	Surface morphology of ZnO	14
2.5	Optical property of ZnO	15
2.5.1	Photoluminescence of ZnO	15
2.5.2	Raman Scattering	17
2.5.3	Effects of annealing on morphology and optical properties of ZnO	18
2.6	Bacteria structure	19
2.6.1	Oral *Streptococcus* bacterium	20
2.6.2	*Streptococcus sobrinus* and *Streptococcus mutans*	21
2.7	Antibacterial activity of ZnO	22
2.8	Minimum inhibition concentration (MIC) and Minimum bacteriacidal concentration (MBC)	24
2.9	Human Gingival Fibroblast (HGF)	26
2.10	Toxicity of ZnO particles	27
2.11	Zinc oxide eugenol (ZOE)	28
2.11.1	Compressive strength of zinc oxide eugenol (ZOE)	29
2.11.2	Hardness of zinc oxide eugenol (ZOE)	31
2.11.3	Simulated body fluid (SBF)	31
2.12	Summary	32

CHAPTER 3 - METHODOLOGY

3.1	Introduction	33
3.2	Synthesis of ZnO	33
3.3	Experimental framework	35
3.4	Field emission scanning electron microscope (FESEM)	36
3.5	Energy filtered transmission electron microscopy (EFTEM)	38
3.6	X-ray diffraction (XRD)	40
3.7	Photoluminescence spectroscopy (PL)	42
3.8	Raman spectroscopy	45
3.9	Dynamic Light Scattering (DLS)	46
3.10	Annealing of ZnO	49
3.11	Preparation of zinc oxide eugenol (ZOE)	50
3.12	Antibacterial study	51
3.12.1	Minimum inhibition concentration (MIC) and Minimum bacteriacidal concentration (MBC) of ZnO	53
3.12.1(a)	MIC determination using MIC test strip	55
3.12.2	Antibacterial study of ZnO	57
3.12.3	Antibacterial study of zinc oxide eugenol (ZOE)	58
3.12.4	Fixation of bacteria for field emission scanning electron microscopy (FESEM) viewing	60
3.13	Cytotoxicity test	61
3.13.1	Cytotoxicity of ZnO particles	66
3.13.2	Cytotoxicity of zinc oxide eugenol (ZOE)	67
3.14	Reactive oxygen species detection (ROS)	69

3.14.1 Reactive oxygen species (ROS) detection for antibacterial activity 70

3.15 Compression strength of zinc oxide eugenol (ZOE) 71

3.16 Vickers Hardness of zinc oxide eugenol (ZOE) 74

3.17 Simulated Body Fluid (SBF) 76

3.17.1 UV-Visible Spectroscopy 77

3.17.2 Atomic Absorption Spectroscopy (AAS) 78

3.18 Summary 81

CHAPTER 4 - EXPERIMENTAL RESULTS

4.1 Introduction 82

4.2 Morphological and elemental mapping analysis 82

4.3 X-ray diffraction (XRD) analysis 91

4.4 Photoluminescence (PL) spectroscopy 96

4.5 Raman spectroscopy 100

4.6 Particle size analyzer using dynamic light scattering (DLS) 103

4.7 Antibacterial properties of ZnO 106

4.7.1 Minimum inhibition concentration (MIC) and minimum bacteriacidal concentration (MBC) of ZnO on *Streptococcus sobrinus* and *Streptococcus mutans* 106

4.7.2 Minimum inhibition concentration (MIC) on *Streptooccus sobrinus* and *Streptococcus mutans* using test strip of Penicillin G 109

4.7.3 Percentage inhibition after 24 h 112

4.7.3 (a) *Streptococcus sobrinus* 112

4.7.3 (b) *Streptococcus mutans* 116

4.7.4 Reactive oxygen species (ROS) detection 119

4.8 Antibacterial properties of zinc oxide eugenol (ZOE) 122

4.9 Cytotoxicity of ZnO on human gingival fibroblast (HGF) 127

4.10 Cytotoxicity of zinc oxide eugenol (ZOE) on human gingival fibroblast (HGF) 134

4.11 Compression strength of zinc oxide eugenol (ZOE) 138

4.12 Vickers hardness of zinc oxide eugenol (ZOE) 141

4.13 Simulated body fluid (SBF) and release profile studies 143

4.13.1 Morphological analysis of zinc oxide eugenol (ZOE) by using FESEM 143

4.13.2 Eugenol detection 145

4.13.3 Atomic absorption spectroscopy (AAS) 146

4.14 Summary 148

CHAPTER 5 - ANALYSIS AND DISCUSSIONS

5.1 Introduction 149

5.2 Key factors of antibacterial activity 149

5.3 Proposed mechanism of antibacterial activity of ZnO 150

5.4 Proposed mechanism of cytotoxicity of ZnO on human gingival fibroblast (HGF) 155

5.5 Zinc oxide eugenol (ZOE) setting 158

5.5.1 Effect of particle size and morphology of ZnO on zinc oxide eugenol (ZOE) cytotoxicity 161

5.5.2 Effect of ZnO surface defect on toxicity 165

5.5.3 Effects of particle size on mechanical strength 166

CHAPTER 6 - CONCLUSIONS AND FUTURE DIRECTIONS

6.1 Conclusions 168

6.2 Future research directions and recommendation 171

REFERENCES 173

APPENDICES

LIST OF PUBLICATIONS 208

LIST OF TABLES

		Page
Table 2.1	Function of main components in a bacterial cell.	20
Table 2.2	Reported MIC value of *S.sobrinus* and *S.mutans* from other researchers.	26
Table 2.3	Classification of ZOE according to ISO 3107	29
Table 2.4	Previously reported values for compression strength of ZOE by researchers	30
Table 3.1	List of chemicals in solution *X* and *Y* to prepare SBF	76
Table 4.1	Lattice constant *c* and *a* , crystallite size, strain and stress of all ZnO and ZOE	95
Table 4.2	Phonon modes of ZnO and ZOE	103
Table 4.3	Colonies formed on blood agar after 30 minutes treatment of ZOE-A, ZOE-B and ZOE-K on *S. sobrinus*	123
Table 4.4	Colonies formed on blood agar after 24 h treatment of ZOE-A, ZOE-B and ZOE-K on *S. sobrinus*	124
Table 4.5	Colonies formed on blood agar after 30 minutes treatment of ZOE-A, ZOE-B and ZOE-K on *S. mutans*	125
Table 4.6	Colonies formed on blood agar after 24 h treatment of ZOE-A, ZOE-B and ZOE-K on *S. mutans*	126

LIST OF FIGURES

		Page
Figure 1.1	Structure of human teeth	3
Figure 1.2	Class of tooth decay	4
Figure 2.1	Hexagonal wurtzite crystal structure of ZnO	13
Figure 2.2	Ilustration of electron transitions from conduction band (CB) to valence band (VB) that emit luminescence in different range of wavelength	16
Figure 2.3	Structure of a typical bacteria cell	19
Figure 2.4	Ilustration of replication, transcription and translation during cell growth by catalytic and genetic functions	21
Figure 2.5	Schematic diagram of gram-positive cell wall	22
Figure 2.6	Type of oxygen species. The red marks indicated an unpaired electron	23
Figure 2.7	Illustration on MIC and MBC determination by broth dilution technique	25
Figure 2.8	Structure of typical human cell	27
Figure 3.1	Experimental framework	34
Figure 3.2	Schematic diagram of the interaction of an electron beam with the sample and the signals generated	37
Figure 3.3	(a) FESEM instrumentation [Jeol.usa.inc]; (b) FESEM FEI Nova NanoSEM 450	37
Figure 3.4	(a) A schematic diagram of parts in EFTEM; (b) EFTEM Zeiss Libra 120	39
Figure 3.5	Diffraction of X-rays in a crystalline material	41
Figure 3.6	(a) typical XRD experiment; (b) PANanalytical X'pert Pro XRD	42

Figure 3.7	(a-d) Radiative recombination processes: (a) band to band; (b) donor to valenceband; (c) conduction band to acceptor; (d) donor to acceptor; (e) Non-radiative recombination via an intermediate state. The E_d, E_a and E_i indicate the donor, acceptor and intermediate states, respectively	43
Figure 3.8	Typical experimental setup for PL measurements	44
Figure 3.9	A unit of Horiba Jobin Yvon HR-800UV, Photoluminescence and Raman spectroscopy.	45
Figure 3.10	Schematic diagrams of Rayleigh scattering, Stokes Raman scattering and Anti-stokes Raman scattering [96]. The v_i and v_f represent the initial and final states, respectively	46
Figure 3.11	(a) Malvern Zetasizer NanoZS to measure the particle size and Zeta potential of ZnO-A, ZnO-B, ZnO-K and ZnO-Ax, (b) the disposable folded capillary cell cuvette for measurement particle size and zeta potential	47
Figure 3.12	(a) The schematic diagram of dynamic light scattering in Malvern Zetasizer NanoZS; (b) example of particle size distribution from a suspension	48
Figure 3.13	Annealing tube furnace LENTON VTF/12/60/700	49
Figure 3.14	Zinc oxide eugenol (ZOE), before and after set (hardened) in acrylic mold	51
Figure 3.15	(a) *S. sobrinus* (b) *S. mutans* cultures on sheep-blood agar; (c) adjusted 0.5 McFarland bacteria suspension in peptone water using (d) BD Spectrometer	52
Figure 3.16	Diagram of 96 microtiter plate for MIC and MBC determination using broth microdilution	54

Figure 3.17	The BIOMIC V3 equipment for calculating number of colony on agar plate	55
Figure 3.18	Penicillin G strip on *S. sobrinus* and *S. mutans* for MIC determination.	56
Figure 3.19	Versamax, a spectrophotometer equipment to measure optical density (OD) of microtiter plate.	58
Figure 3.20	ZOE pellets in the bacterial suspensions	59
Figure 3.21	(a) DMEM, ATCC 30-2002, (b) penicillin-streptomysin, (c) Fetal bovine serum (FBS) and; (d) the ATCC CRL 2014 HGF-1 cell line	63
Figure 3.22	(a) A haemacytometer for counting the number of cells; (b) trypan blue stains	63
Figure 3.23	A light microscope Olympus CKX41	63
Figure 3.24	(a) HGF cell in T75 flask; (b) HGF cells in 96 microtiter plate; (c) CCK-8; (d) BMG FLUOstar, a spectrophotometer to measure OD at 450nm	64
Figure 3.25	The interaction between CCK-8 chemical (WST-8) and cells to generate formazon dye for determining cell viability.	65
Figure 3.26	ROS detection by H_2DCFDA	70
Figure 3.27	(a) BMG FLUOstar Omega fluorescence spectroscopy; (b) Incubator at 37 ºC.	71
Figure 3.28	(a) The compression equipment of Shimadzu Autograph AG-X plus 20 kN (b) the ZOE pellet on the compression plate	72
Figure 3.29	The harden pellets of (a) ZOE-A, (b) ZOE-B (c) ZOE-K and (d) ZOE-(e) the schematic diagram of the ZOE pellet, (e) stainless steel mold with 4 mm diameter and 6 mm height	73

Figure 3.30	A schematic diagram of Vickers indentation and measurement of impression diagonal	74
Figure 3.31	The FIE VM-50 of Vickers hardness equipment (b) the diamond indentation on specimen surface (c) the ZOE pellet in acrylic mould of 5 mm diameter and 2 mm height	75
Figure 3.32	(a) Cary Series UV-Vis-NIR spectroscopy by Agilent Technologies; (b) schematic diagram of UV-Vis	78
Figure 3.33	Atomic absorption Spectrometer of Perkin Elmer AAnalyst400	80
Figure 3.34	(a) Zn standard solution of 1000 ppm for AAS measurement and (b) the dilution of Zn standard solution.	80
Figure 4.1	FESEM and EDX images of (a) ZnO-A, (b) ZnO-B (c) ZnO-K and (d) ZnO-Ax	84
Figure 4.2	TEM images and the frequency of particle size taken from hundred images for (a) ZnO-A, (b) ZnO-B, (c) ZnO-K and (d) ZnO-Ax	86
Figure 4.3	Zinc and oxygen elemental mapping of (a) ZnO-A, (b) ZnO-B, (c) ZnO-K and (d) ZnO-Ax	88
Figure 4.4	FESEM and EDX images of (a) ZOE-A, (b) ZOE-B, (c) ZOE-K and (d) ZOE-Ax	90
Figure 4.5	XRD patterns for, (a) ZnO-A, ZnO-B and ZnO-K; (b) ZOE-A, ZOE-B and ZOE-K	93
Figure 4.6	PL spectra of ZnO-A, ZnO-B, ZnO-K and ZnO-Ax at room temperature. The inset shows green luminescence of all ZnO	99
Figure 4.7	PL spectra of ZOE-A, ZOE-B, ZOE-K and ZOE-Ax at room temperature	99

Figure 4.8	Raman spectra of ZnO-A, ZnO-B, ZnO-K and ZnO-Ax	102
Figure 4.9	Raman spectra of ZOE-A, ZOE-B, ZOE-K and ZOE-Ax	102
Figure 4.10	The graphs of size distribution (nm) for all ZnO powder	105
Figure 4.11	The MIC and MBC of ZnO-A, ZnO-B, ZnO-K and ZnO-Ax on *S. sobrinus*	107
Figure 4.12	The MIC and MBC of ZnO-A, ZnO-B and ZnO-K on *S. mutans*	109
Figure 4.13	MIC test strip of (a) *S. sobrinus* at 0 h; (b) *S. mutans* at 0 h; (c) *S.sobrinus* at 24 h and; (d) *S.mutans* at 24 h	110
Figure 4.14	Number of colony at MIC 0.156 mM for *S. sobrinus* and *S. mutans*	111
Figure 4.15	Percentage inhibition of ZnO-A, ZnO-B, ZnO-K and ZnO-Ax on *S. sobrinus* at 0.5-2 mM. Plot represents the average of percentage inhibition ± *SD* (*n*=3, **p*<0.05)	113
Figure 4.16	FESEM images with EDX data for untreated and treated with *S. sobrinus* after 24 h at 2mM; (a,f) untreated; (b,g) ZnO-A; (c, h) ZnO-B; (d, i) ZnO-K and (e,j) ZnO-Ax	115
Figure 4.17	Percentage inhibition of ZnO-A, ZnO-B, ZnO-K and ZnO-Ax on *S. mutans* at 0.5-2 mM. Plot represents the average of percentage inhibition ± *SD* (*n*=3, **p*<0.05)	117
Figure 4.18	FESEM images with EDX data for untreated and treated with *S. mutans* after 24 h at 2mM; (a,f) untreated; (b,g) ZnO-A; (c, h) ZnO-B; (d, i) ZnO-K and (e,j) ZnO-Ax	118

Figure 4.19	Percentage of fluorescence for control and ZnO treated at 0.5-2 mM on *S.sobrinus* and *S. mutans*. Plots represent average percentage of fluorescence ± *SD* (*n*=3, **p*<0.05)	121
Figure 4.20	Colony count (CFU/mL) for antibacterial test of ZOE-A, ZOE-B, ZOE-K and ZOE- at 10 min, 30 min and 24 h for; (a) *S. sobrinus* and ; (b) *S. mutans*	127
Figure 4.21	Percentage of cell viability of HGF for ZnO-A, ZnO-B, ZnO-K and ZnO-Ax at 0.5, 1.0 1.5 and 2.0 mM. Plots represents the average percentage of cell viability ± SD (*n* =5, **p*>0.05)	129
Figure 4.22	Microscopic images of HGF cells for untreated (control) and treated with ZnO-A and ZOE-A after 72h	130
Figure 4.23	Microscopic images of HGF cells for untreated (control) and treated with ZnO-B and ZOE-B after 72h	131
Figure 4.24	Microscopic images of HGF cells for untreated (control) and treated with ZnO-K and ZOE-K after 72h	132
Figure 4.25	Microscopic images of HGF cells for untreated (control) and treated with ZnO-Ax and ZOE-Ax after 72 h	133
Figure 4.26	FESEM images of ZOE and EDX after 24 h immersion; (a,e) ZOE-A, (b,f) ZOE-B, (c,g) ZOE-K and (d,h) ZOE-Ax	135
Figure 4.27	Percentage of cell viability of HGF cell after 72 h treatment with ZOE-A, ZOE-B, ZOE-K and ZOE-Ax. Plots represent the average percentage of viable cells ± *SD* (*n* = 5, **p*>0.05)	137
Figure 4.28	The compression strength of ZOE-A, ZOE-B, ZOE-K and ZOE-Ax. Plots represent the average of compression strength ± SD (*n* = 7, **p* < 0.05)	141

Figure 4.29	The Vickers hardness value for ZOE-A, ZOE-B, ZOE-K and ZOE-Ax. Plot represents the average vickers hardness ± *SD* (*n* = 5, **p* <0.05)	142
Figure 4.30	The FESEM images of ZOE-A, ZOE-B and ZOE-K before immersion (0 day) and after immersions at 1, 3, 7, 14 and 21 days.	144
Figure 4.31	Percentage of eugenol release of ZOE-A, ZOE-B, ZOE-K and ZOE-Ax in SBF solution at 0, 1, 3, 7, 14, and 21 days	146
Figure 4.32	Graph of AAS for Zn ion release at 1, 3, 7, and 14 and 21 days. Plots represent average ± *SD*	147
Figure 5.1	A schematic diagram of ROS generations by electron hole pairs	151
Figure 5.2	Metal ion mechanism that induce ROS in antibacterial activity	154
Figure 5.3	Summary of factors influence the release elements and effect ROS generation	155
Figure 5.4	Chemical structure of ZnO and eugenol mixing that produce a chelate of zinc eugenolate	159
Figure 5.5	The manipulating factors of ZOE setting.	160
Figure 5.6	Hydrolysis by water molecules on the surface of ZOE matrix.	162
Figure 5.7	Schematic diagram on different morphology and particle size of ZnO that affect the leached element from the ZOE matrix.	163

LIST OF ABBREVIATIONS

ATCC	American Type Culture Collection
AAS	Atomic Absorption Spectroscopy
CCK-8	Cell counting kit-8
CB	Conduction band
CFU	Colony forming unit
CLSI	Clinical Laboratory standard institute
CO_2	Carbon dioxide
DLS	Dynamic light scattering
DMEM	Dulbecco's Modified Eagle Medium
DNA	Deoxyribonucleic acid
EBA	orto-etoxy benzoic acids
EDX	Energy dispersive X-ray
EFTEM	Energy filtered transmission electron microscopy
ESI	Electron spectroscopy imaging
ehp	Electron holes pairs
Eq	Equation
eV	Electron volt
FBS	Fetal bovine serum
FESEM	Field emission scanning electron microscopy
GL	Green luminescence
HGF	Human Gingival Fibroblast
HV	Vickers hardness number
ISO	International organization for standadization
LO	Longitudinal optical

MBC	Minimum bactericidal concentration
MIC	Minimum inhibition concentration
mL	Mililitre
MMA	methyl methacrylate
MTCC	Microbial Type Culture Collection
NBE	Near band edge
NPs	Nanoparticles
O	Oxygen
OD	Optical density
PBS	Phosphate buffer saline
pen-strep	penicillin-streptomycin
PL	Photoluminescence
ppm	Parts per million
RNA	Ribonucleic acid
ROS	Reactive oxygen species
SBF	Simulated body fluid
SPSS	Statistical Package for the Social Science
S. mutans	*Streptococcus mutans*
S. sobrinus	*Streptococcus sobrinus*
TO	Transverse optical
TSB	Trypticase soy broth
VB	Valence band
Vo	Oxygen vacancy
XRD	X-ray diffraction
Zn	Zinc

Zn_i	Zinc interstitial
ZnO	Zinc oxide
ZOE	Zinc oxide eugenol

LIST OF SYMBOLS

a	Basal plane lattice constant
c	Uniaxial lattice constant
d	Lattice plane distance
D	Crystallite size
E	energy
H_2O_2	Hydrogen peroxide
hkl	Miller indices
M	Means
n	Statistical n-trial
$\cdot O_2^-$	Superoxide anion
·OH	Hydroxyl radical
p	Statistical p-value
SD	Standard deviation
t	Independent t-test value
β	full width at half maximum (FWHM)
Γ	Wurtzite structure optical phonons
ε_{zz}	Strain
θ	Scattering angle
λ	wavelength
σ	Stress

KESAN STRUKTUR ZINK OKSIDA TERHADAP PELBAGAI CIRI EUGENOL ZINK OKSIDA YANG DIGUNAKAN DALAM PERGIGIAN

ABSTRAK

Objektif utama tesis ini adalah untuk mengkaji kesan struktur ZnO terhadap ciri pelbagai ciri eugenol zink oksida (ZOE) yang digunakan dalam pergigian. ZnO-A (berbentuk rod), ZnO-B (berbentuk plat), ZnO-Ax (penyepuhlindapan oksigen pada 700 ºC) dan sampel komersial ZnO-K (pelbagai bentuk) mewakili empat jenis serbuk ZnO yang mempunyai morfologi berbeza. ZnO ini digunakan untuk menyediakan ZOE dan dilabel sebagai ZOE-A, ZOE-B, ZOE-K dan ZOE-Ax. *Streptococcus sobrinus* dan *Streptococcus mutans* digunakan untuk ujian aktiviti antibakteria. Sel HGF (human gingival fibroblast) digunakan untuk ujian ketoksikan. Pencirian sifat morfologi, struktur dan optik dilakukan bagi semua ZnO dan ZOE. Elektron mikroskop menunjukkan kandungan oxygen yang tinggi pada permukaan rod ZnO-Ax, diikuti oleh ZnO-A, ZnO-B dan ZnO-K. Taburan saiz partikel dari serakan cahaya dinamik untuk ZnO-A ialah 21.82 nm (91.9%), 52.21 nm (85.7%) untuk ZnO-B, 1140 nm (100%) untuk ZnO-K dan 20.08 nm (95.3%) untuk ZnO-Ax. Berdasarkan spektrum fotoluminesen, terdapat dua puncak untuk semua ZnO iaitu pada kawasan ultra-ungu (UV) dan luminesen hijau (GL). Walaubagaimanpun, keamatan puncak dominan pada kawasan UV pada semua ZOE adalah sangat rendah berbanding ZnO, manakala puncak GL hampir tidak kelihatan. Keputusan ini menunjukkan kecacatan pada setiap jenis ZnO telah hampir lenyap setelah dicampurkan dengan eugenol disebabkan oleh proses hidrolisis. Aktiviti antibakteria ZnO diuji keatas *S.sobrinus* dan *S. mutans* pada 0.5-2mM. Bagi *S. sobrinus*, peratusan perencatan pada 2.0 mM adalah 82.32% (ZnO-A), 78.54% (ZnO-B), 55.30% (ZnO-K) dan 89.0% (ZnO-Ax). Peratusan perencatan yang lebih tinggi dapat dilihat pada *S. mutans* dengan 88.55 %

(ZnO-A), 86.33% (ZnO-B), 77.98% (ZnO-K) and 97.9% (ZnO-Ax). Perencatan ini disebabkan oleh ROS yang dijana oleh pasangan lubang-elektron, paras oksigen pada permukaan ZnO dan ion Zn yang terlarut . Oleh itu, saiz partikel yang lebih kecil pada ZnO-Ax mengalami lebih banyak perencatan disebabkan oleh nisbah permukaan dan isipadu yang lebih luas untuk menjana ROS. Kesan ketoksikan ZnO diuji terhadap sel normal HGF pada kepekatan yang sama seperti antibakteria iaitu 0.5-2.0 mM. Pada 2.0 mM, sel hidup untuk ZnO-Ax adalah 65.57% manakala ZnO-A (72.18%), ZnO-B (74.24%) dan ZnO-K (69.49%). Perbezaan terhadap kesan toksik ini berlaku akibat daripada perbezaan paras oksigen dan saiz partikel, kerana ia mempunyai luas permukaan yang lebih luas. Keadaan ini membolehkan lebih banyak ROS dijana dan membawa kepada kesan toksik yang lebih tinggi terhadap sel berbanding saiz partikel yang lebih besar. ZOE-Ax adalah kurang toksik terhadap HGF berbanding ZOE-A, ZOE-B dan ZOE-K kerana ikatan matriks ZOE yang kuat dan kurang element terlesap (Zn^{2+} dan eugenol). Selepas 72 jam, pada 40% ekstrak ZOE-Ax, sel hidup adalah 82.01%, manakala untuk ZOE-A adalah 72.24%, ZOE-B adalah 67.32% dan 51.41% untuk ZOE-K. Kawasan permukaan yang luas pada ZnO-Ax memberikan lebih permukaan untuk bertindak balas dengan eugenol dan memberikan ikatan kekunci antara elemen yang lebih kuat. Kekuatan mampatan ZOE-AX (43.19 MPa) adalah lebih tinggi daripada ZOE-A (33.6 MPa), ZOE-B (28.1 MPa) dan ZOE-K (17.88 MPa). Ini kerana ikatan kekunci oleh partikel kecil adalah lebih baik dan menghalang elemen dari terlesap keluar dan dapat mengurangkan janaan ROS semasa aktiviti ketoksikan.

EFFECTS OF ZINC OXIDE STRUCTURES ON VARIOUS PROPERTIES OF ZINC OXIDE EUGENOL USED IN DENTISTRY

ABSTRACT

The main objective of this thesis is to investigate effects of ZnO structure on various properties of zinc oxide eugenol (ZOE) used in dentistry. ZnO-A (rod shape), ZnO-B (plate shape), ZnO-Ax (oxygen annealed at 700 °C), and a commercial sample ZnO-K (multi-shape) represent four types of with different morphology zinc oxide (ZnO) powders. These ZnO powders were used to prepare different ZOEs labeled as ZOE-A, ZOE-B, ZOE-K, and ZOE-Ax. *Streptococcus sobrinus* and *Streptococcus mutans* were used to observe antibacterial activities in this study. Human gingival fibroblast (HGF) cell line was used for cytotoxicity test. Morphological, structural, and optical properties were characterized for all ZnO and ZOE samples. Electron microscopy revealed high contents of oxygen elements on particle surfaces of ZnO-Ax, followed by ZnO-A, ZnO-B, and ZnO-K. Distributed particle size from dynamic light scattering of ZnO-A measured 21.82 nm (91.9%), 52.21 nm (85.7%) for ZnO-B, 1140 nm for (100.0%) ZnO-K, and 20.08 nm (95.3%) for ZnO-Ax. Based on photoluminescence spectra, two peaks for all ZnO at ultraviolet (UV) and green luminescence (GL) regions were observed. However, intensity of the dominant peak at the UV region was extremely low in all ZOE compared with that in ZnO, and GL was almost diminished. Results imply loss of defects contained in each type of ZnO structures after mixing with eugenol because of hydrolysis. Antibacterial activities of all ZnO samples on *S. sobrinus* and *S. mutans* were studied at 0.5–2.0 mM. For *S. sobrinus*, inhibition percentages at 2.0 mM reached 82.32% (ZnO-A), 78.54% (ZnO-B), 55.30% (ZnO-K), and 89.0% (ZnO-Ax). High inhibition percentages of 88.55% (ZnO-A), 86.33% (ZnO-B),

77.98% (ZnO-K), and 97.9% (ZnO-Ax) were observed for *S. mutans* at 2.0 mM. Such inhibition was due to reactive oxygen species (ROS) generated by electron–hole pairs, increased oxygen level on ZnO surface, and dissolved Zn ions. Therefore, small particle size in ZnO-Ax results in significant inhibition because of large surface area to volume ratio for ROS generation. Cytotoxic effect of ZnO was tested on normal HGF cell line at the same concentration with antibacterial testing (0.5–2.0 mM). At 2.0 mM, low percentage of viable cells for ZnO-Ax (65.57%) indicates slightly higher toxicity than that of ZnO-A (72.18%), ZnO-B (74.27%), and ZnO-K (69.49%). Different toxicity effects were due to differences in oxygen levels and particle sizes, with small particle size associated with high surface areas. This condition allows generation of more ROS, causing additional toxicity effects on cells in comparison with that in large particle size. ZOE-Ax is less toxic in HGF compared with ZOE-A, ZOE-B, and ZOE-K because of strong adhesion bond of formed ZOE matrix and less amount of leached elements (Zn^{2+} and eugenol). After 72 h and at 40% ZOE-Ax extract, viable cells reached 82.01%, whereas those of ZOE-A, ZOE-B, and ZOE-K totaled 72.24%, 67.32%, and 51.41%, respectively. Small particle size and high oxygen level of ZnO-Ax provided a large surface area for eugenol reaction. Thus, strong adhesion bonds formed. Compression strength of ZOE-Ax totaled 43.19 MPa, which is higher than those of ZOE-A (33.6 MPa), ZOE-B (28.1 MPa), and ZOE-K (17.88 MPa). This good compression strength (ZOE-Ax) results from good adhesion bond by small particle size; compression strength will prevent leaching of ZnO and eugenol element when in contact with aqueous solutions. Thus, decrease in leaching element will lead in decreased ROS generation in toxic activities.

CHAPTER 1

INTRODUCTION

1.1 Introduction

Zinc oxide (ZnO) is an outstanding material from group II–IV semiconductor materials. Given the wide bandgap properties that are essential in optoelectronic devices, such as light-emitting diodes, photovoltaics, ultraviolet (UV) detector, and gas sensor [1,2], ZnO semiconductors have attracted numerous studies in recent years. Research and development have been exploring and manipulating ZnO for decades to improve its properties and efficiency and thus increase its value in industries.

Interestingly, ZnO applications are not only employed in industrial and engineering fields but are also used for biomedical purposes. This semiconductor material exhibits antibacterial effects, which attracted raised considerable attention among researchers [3,4]. To date, ZnO is widely used for medical purposes, such as dental materials, cosmetics, medicated powder, mouthwash, toothpaste, sunblock cream, calamine lotion, and as food packaging [4,5].

Essentially, when applied to human skin or inserted into the human body, actual mechanism and interactions of ZnO at the cellular level remain unelucidated. Despite significant progress in medical applications, toxicity level released by ZnO has been a recent matter of concern among researchers. Thus, identifying appropriate dose of ZnO in each application bears importance to ensure effectiveness at optimum level with minimum symptoms of side effects or allergies.

1.2 ZnO eugenol

ZnO eugenol (ZOE) comprises ZnO and eugenol mixture, with ZnO powders accounting for 80%–90%, and the remaining components include eugenol-bonded resin consisting other chemical such as zinc acetate, zinc acetate,resin and inert oil [6]. In dentistry, ZOE is used as temporary dental filler, liner, and base [4]. To date, several types of commercial products of ZOE are available in the market with different types and categories. For example, ZOE is available in several forms, namely, paste–paste, paste–liquid, or powder–liquid form. With the advancement of technology and research, ZOE is classified into two types according to ISO 3107:2011 [7]:

- Type I: for temporary cementation
- Type II: for bases and temporary restorations.

According to the latest classification of ISO 3107:2011, this study focuses on type II ZOE. Figure 1.1 shows the structure of human tooth, where enamel and dentin are found in the crown section. As depicted in Fig. 1.2, different types of tooth cavities are divided into several classes and treatments. Class I cavity is a decay involving enamel and dentin areas only and does not reach the pulp. This condition is treated by indirect pulp capping, wherein ZOE is not directly placed into the pulp, but only in tooth cavity.

Eugenol ($C_{10}H_{12}O_2$) is an essential oil from clove oil. Recorded properties of eugenol include an alkaline pH of 7 [8] and molecular weight of 164.2 g/mol. Eugenol naturally occurs in liquid form with pale yellow color. It have been reported that eugenol have antibacterial effects by inducing cell lysis through leakage of protein and lipid in the cell membrane [11]. Moreover, eugenol have anti-inflammatory effects where it can supress the expression of cyclooxygenase II enzymes. Cyclooxygenase is a catalayse the

formation of prostaglandin (in promoting inflammation) [11]. However, eugenol alone can produce local irritative and adverse reactions to periapical tissues [12,13]. This side effect has increased practitioners' awareness to this type of dental material. Therefore, to decrease allergic reactions in sensitized patients, minimum leaching of elements from ZOE are required without affecting antibacterial properties. ZnO is the major ingredient in ZOE. Thus, ZnO properties can affect ZOE characterization. Different ZnO structures may affect release of elements in ZOE, eventually influencing antibacterial activity and cytotoxicity effects on normal cells.

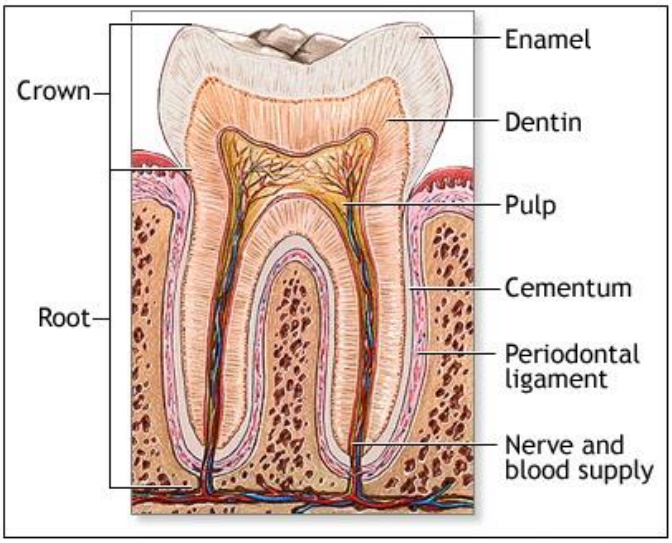

Figure 1.1: Structure of human teeth [14]

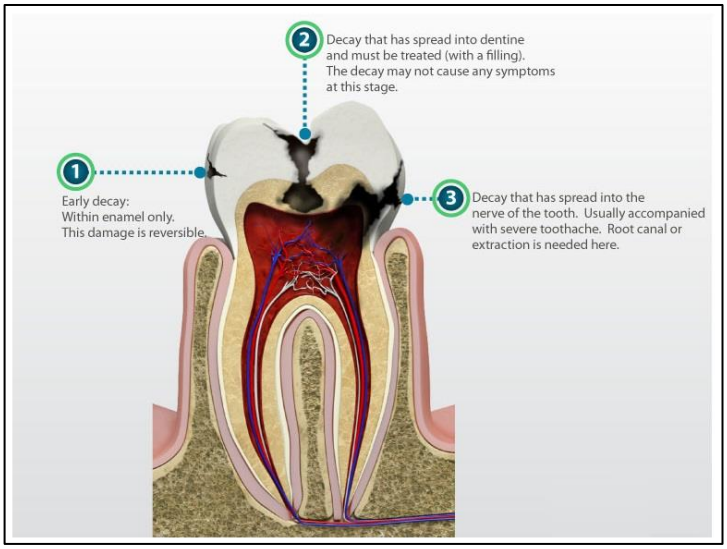

Figure 1.2: Classes of tooth decay [15]

When ZOE is exposed to oral fluids, eugenol will diffuse into the oral fluid and will be substituted with water, leading to hydrolysis of ZnO eugenolate. ZOE will disintegrate and release ZnO and eugenol. This function is important in antibacterial activity because cavities are normally caused by bacteria. When ZOE is administered to cavities, it will inhibit bacterial growth and decrease potential caries underneath.

Naturally, pH of ZOE approximates 7, and it is currently considered a less irritating pulp dental material [10]. Thus, ZOE can be used in deep cavities. Given that ZOE will release eugenol and ZnO into cavities, it will cause obtundent effects to the aching tooth. ZOE will not shrink in size after application to cavities. Thus, it will strongly bond to the cavity edge and prevent microleakage. Microleakage is a condition wherein bacteria can enter cavities and irritate the pulp because of poor adhesive or bonding of ZOE to cavity edge [10,13].

For all ZOE types, the principle of setting reaction is essentially the same. However, ZOE properties can be altered by physical properties of ZnO, specifically,

particle size [15]. Particle size mainly affects strength and setting time. However, few studies reported antibacterial and cytotoxic activities of ZOE with different particle sizes and morphologies. Therefore, this study emphasizes effects of morphology and particle size of ZnO in ZOE on antibacterial and cytotoxic activities. Compression strength and hardness value of ZOE pellet were evaluated. Chapter 5 studies and discusses effects of particle size and oxygen level of ZnO structure on ZOE hardness and compression strength.

1.3 Oral bacteria

Thousands of species of microorganisms (spp.) exist in the human oral cavity, and each species exhibits different functions that can cause many types of oral problems or diseases. Species that can cause diseases are called pathogens. For example, *Streptococcus sobrinus* and *Streptococcus mutans* from *Streptococcus* species (*Streptococcus* spp.) are pathogenic [18]. These bacteria have been identified to be root causes of tooth cavity, which may lead to severe diseases and large cavities when they continually exist in oral cavity for long periods. When cavities are not treated immediately, these bacteria may intrude blood vessels via the tooth pulp and cause severe pain and bacterial infection [18].

Both *S. sobrinus* and *S. mutans* are Gram-positive bacteria characterized by a thick layer of peptidoglycan, which can accommodate crystal violet staining and provides purple color to the bacteria under microscopy during Gram staining.

1.4 Background of the study

The main originality of this research lies in experimental studies of antibacterial and cytotoxic effects of ZOE produced from different ZnO structures and oxygen-annealed ZnO. Through this study, morphological dependence of antibacterial and toxicity behaviors toward the same concentrations of ZnO is reported. Effects of oxygen level on ZnO structure causes good antibacterial activity and lessens cytotoxic effects of ZOE. To date, our work pioneers in reporting effects of different ZnO structures on morphology and structural and optical properties of ZOE; antibacterial and cytotoxic activities were also studied. In general, few studies reported MIC values of ZnO structures in cariogenic bacteria. Thus, with the obtained information on MIC, ZnO usage in dental applications can be supported by in vitro studies of normal human cell.

Eugenol is highly alkaline in nature and toxic on several cell lines at a pH of 7.4 [10]. However, results from this study show the opposite for ZOE. ZOE toxicity has been investigated on HGF cell line by focusing on elements leached by ZOE. The present study reveals uniqueness of ZOE matrix formation during mixing and adhesion behavior between different morphologies of ZnO structure and eugenol.

Results of this research have led to good understanding of ZOE properties. ZOE synthesized in the laboratory using ZnO structure can compete with commercial ZOE availed in markets in terms of toxicity level on HGF cell line and compression strength and hardness value of ZOE pellets when using ZnO with small particle size in mixing. Mechanical strength increases ZOE durability as temporary restorative material.

1.5 Problem statement and novelty of the studies

Zinc oxide eugenol is a material that have been used for decades. Many researchers have been developing new ZOE with added chemicals or polymer to reinforced the cement's mechanical properties. In example, current commercial reinforced ZOE that available in the market have added orto-etoxy benzoic acids (EBA) and/or methyl methacrylate (MMA). It is known that EBA and MMA can increased the compression strength. Unfortunately, both EBA and MMA posses high potential toxicity as described by Leggat (2003) [20] and Fujisawa et.al (2003) [21]. EBA can cause skin irritation, eye irritation, and respirotory irritation. On the other hand, exposure to MMA can cause toxicity to patients and the dental staff [22]. Occasionally, the exposed area to MMA may suffer hypersensitivity, asthmatic reaction or breathing difficulties, local neurological symtoms, irritant and local dermatological reaction [23]. Thus this study focused on increasing the compression strength without compromising the antibacterial effects and maintaining low toxicity to nomal gingival cell line.

Previous researchers have reported that ZnO NP have high minimum inhibition concentration (MIC) as decribed in section 2.8, and this high MIC is not preferable since it refers to poor bacterial growth inhibition. Apart from that, the toxicity of ZOE must be very low towards periapical tissue. Low mechanical strength is another problem in ZOE material. According to ISO 3107, type II ZOE must have minimum 5 MPa, and other researcher reported around 5-35 MPa as presented in Table 2.4 (chapter 2.11.1). From problems listed above, there is a gap where there is a need for better ZOE in term of high antibacterial effects, low toxicity and high compression strength.

In this project the novelty are the selective toxicity of ZnO and ZOE, where it is highly toxic toward bacteria but less toxic toward normal cell lines. Moreover, investigation on minimum inhibition concentration (MIC) of ZnO were presented, where the low MIC concentration were recorded according to standard procedure CLSI M07-A10 and CLSI M100-S24 (the details will be discussed in section 3.11.1). On top of that, the ZOE compression strength were increased by ZnO surface state modofication, without adding other potential toxicity chemicals or polymers.

1.6 Objectives of the study

The main aims of this research encompass the following:

- To investigate the morphology, structural and optical properties of four types of ZnO structures and prepare ZOE samples
- To determine the minimum inhibition concentration (MIC) of ZnO structures on *Streptococcus sobrinus* and *Streptococcus mutans* and the antibacterial activity of synthesized ZOE samples
- To investigate the performance of prepared ZOE samples with respect to their toxicity (on Human gingival fibroblast) and physical properties (compression strength and surface hardness)

1.7 Scope of the study

The scope of the study has been determined to ensure that results and discussions fulfill research objectives.

First, the research work focused on undoped ZnO structure produced by French process and as the main material. Two types of ZnO powder were used: ZnO-A and ZnO-B. These ZnO occur naturally in powder form. However, ZnO-A and ZnO-B were converted into a solution or pellet form according to experimental purposes. Another ZnO commercial sample (ZnO-K) was used for comparison. The oxygen-annealed ZnO-A powder (later labeled as ZnO-Ax) was used to study effects of thermal treatment and ZOE properties on ZnO surface. Characterizations of ZnO were limited to its morphological, structural, optical, antibacterial, and cytotoxic analyses.

Second, this research work focused on ZOE as a temporary restoration material. The synthesized ZOE comprises ZnO powder and eugenol-bonded resin. The formulated eugenol-bonded resin was used to standardize the resin, stabilizer, and other small components (~5%) utilized in ZOE mixture. Standardization is important because obtained results only depended on ZnO structures and elimination of unwanted variables. Working temperature and humidity during mixing and powder-to-liquid ratio for ZOE were maintained to reduce variables that can compromise results.

Third, this research also centered on human oral bacteria that are mostly related to tooth cavity. Two types of Gram-positive bacteria from *Streptococcus* spp. were used to investigate MIC and antibacterial activity of ZnO samples. Few techniques were conducted to observe ZnO response on bacteria. These techniques include serial dilution, optical density measurement, and electron microscopy. For ZOE pellets, antibacterial

activity was detected by colony count and not disc diffusion method because of the lack of moisture provided by blood agar during incubation and hemolysis of ZOE. Moisture is important in initiating production of reactive oxygen species (ROS) and inhibiting bacterial growth. Therefore, colony count method was selected to minimize potential interruption caused by method limitations and natural properties of the material itself.

Toxicity evaluation was conducted on normal HGF cell line. This cell line was selected because of its close relation to ZOE application as temporary dental restorative. Cell viability was measured by cell counting kit-8 (CCK-8) assay. This assay is compatible with adherent type of HGF cell line and is suggested by ISO 10993-part 5 [19], which prefers quantitative experiments.

Finally, the physical properties of ZOE was evaluated using compression strength and Vickers hardness. The experimental method for compression strength is in accordance to ISO 3107:2011 [9]. Therefore the physical properties of all ZOE are affects by diffferent size and morphology of ZnO.

1.8 Overview of the study

In general, contents of this dissertation are organized as follows.

Chapter 2 reviews early studies on structural and optical properties of ZnO. However, emphasis will be placed on ZnO application in dentistry as temporary dental restorative of ZOE. This chapter will also present an overview of antibacterial effects and toxicity levels. The main mechanisms involved in antibacterial and toxicity effects proposed by previous researchers are also described.

Chapter 3 concentrates on general principles of each equipment and characterization tools used in this study. Considered factors include sample details, experimental set-up, and operating conditions. Procedures for antibacterial and cytotoxicity tests are also included according to international standards.

Chapter 4 describes thoroughly experimental results, including antibacterial and cytotoxic activities, during characterization of ZnO and ZOE.

Chapter 5 devotes to the effect of ZnO structure on antibacterial and cytotoxic activities. Discussions will elaborate how the same concentration of ZnO can almost kill bacteria but preserved the normal human cell line with high percentages of cell visibility. This chapter will also discuss influence of different morphologies on compression strength and hardness of ZOE.

Finally, Chapter 6 concludes the study. Future recommendations for continuity of this research work are also presented.

CHAPTER 2

LITERATURE REVIEW

2.1 Introduction

This chapter discuss briefly an overview of ZnO applications and its surface and optical properties. Subsequently, we will introduce types of oral bacteria and cell lines, including their anatomical structure. Primary mechanisms involved in antibacterial and cytotoxicity are also addressed. Lastly, this chapter provides information regarding ZOE.

2.2 Application of ZnO

ZnO is a versatile semiconductor material. For many years, this material has been used in various industries, including automotive, cosmetics, food packaging, and dental material [1,3,4,5]. With regard to its wide band gap energy (3.37 eV) and high exciton binding energy (60 meV) at room temperature, extensive techniques have been developed for ZnO production, wherein fabricated structures feature various shapes and nanosizes according to their functions and applications. Some examples include comb, spiral, needles, saws, tubes, belts, wires [24,25,26], and other complicated structures for various special devices, such as near UV lasers, high-efficiency photonic devices, piezoelectric transducer, varistor, and gas sensor [27,28].

Given that this ZnO can inhibit antibacterial growth and exhibits sedative effects, it is used widely in dental materials as the main ZOE component. In principle, ZOE is used as cavity liner, base, and restorative materials because of its general properties that include thermal protection, microleakage prevention, buffer layer of dentinal tubules, and

ability to eliminate postoperative sensitivity [29]. To date, utilization of ZOE as dental material remains relevant despite its use for decades [30].

2.3 Properties of ZnO

ZnO is a binary II–IV compound that displays a hexagonal wurtzite structure. This material possesses a hexagonal and close-packed crystal structure with parameters of a hexagonal unit cell with a= 3.2495 Å and c= 5.2069 Å and density of 5.67 g cm^{-3} [31,32]. In addition to wurtzite, ZnO crystals are also found in cubic structures of zincblende and rock salt. At room temperature, the stable phase of ZnO is wurtzite structure. ZnO zincblende structure is only stable for growth on cubic substrates [33], whereas rock salt can be obtained at relatively high pressure at ~10 GPa [34].

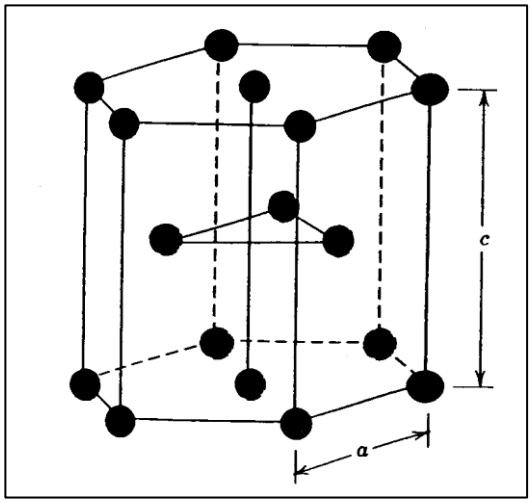

Figure 2.1: Hexagonal wurtzite crystal structure of ZnO

In an ideal wurtzite structure, the ratio of two lattice parameters *a* and *c* of a hexagonal unit cell is $c/a = \sqrt{8/3} = 1.633$. Another internal lattice parameter *u* is defined as the length of bond parallel to the *c*-axis (anion–cation bond length or nearest-neighbor distance) divided by *c* lattice parameter [35]. The basal plane lattice parameter (edge length of basal plane hexagon) is universally depicted by *a*. Axial lattice parameter (unit cell height) is perpendicular to the basal plane and is universally described by *c*. Each sublattice includes four atoms per unit cell, and each kind of atom (group II atom) is surrounded by four atoms of another kind (group VI), or vice versa, which are coordinated at the edges of a tetrahedron [35].

2.4 Surface morphology of ZnO

Many techniques have been developed to fabricate ZnO with various shapes, sizes, and morphology. Examples include sheets, rods, combs, needles, saws, wires, flowers, rings [36,37], tetrapods [38], and other shapes at the nano- and microscale. Each shape particularly provides interesting characteristics in applications because of good optical properties rendered on the material.

Researchers reported that well-aligned ZnO nanowires synthesized by simple physical vapor deposition shows single strong UV emission at 380 nm in photoluminescence (PL) without any green, yellow, or red emission peak observed [39]. Green, yellow, and red emissions in the PL spectrum are attributed to defects caused by a few types of oxygen and zinc vacancies [36,38,39,40]. Kurbanov et al.(2015) reported high-quality tetrapod-like ZnO consisting of four arms synthesized by a modified vapor transport process [38]. This highly uniform tetrapod shape exhibits strong UV emission

in PL spectrum at approximately 390 nm with no familiar green emission detected at 510–580 nm [38]. Flower-shaped ZnO obtained by Umar et al. (2005) [41] showed sharp and strong UV emission at 378 nm, with suppressed broad green emission at 520 nm, indicating good crystal quality and few defects [41]. These fabricated ZnO structures with highly crystalline wurtzite structure can be applied to excellent optoelectronic devices, such as UV laser emitters and super lenses [40]. Defects and impurities detected by PL will be discussed in the following section.

Numerous reports on good optical properties of nanostructure fabrications have been documented [36,38,40,41]. However, few studies have been conducted on application of these nanostructures for biomedical purposes. Therefore, this study focuses on effects of ZnO morphology on antibacterial and toxicity level to demonstrate efficacy and safety characteristics of ZOE as dental material.

2.5 Optical property of ZnO

Optical characteristics are important properties of ZnO. The ability to absorb and emit photons can be measured by dedicated instruments. In principle, energy band gap and defects can be measured using PL spectroscopy, whereas phonons can be detected by Raman scattering. Therefore, in this study, PL and Raman spectroscopy were used to probe optical properties of ZnO structure.

2.5.1 Photoluminescence of ZnO

PL is an intrinsic optical property widely reported for ZnO. Band-to-band transition of an electron will emit strong emission peak in the UV region. Green emission is another generally occurring peak and is proposed to be related to oxygen vacancies,

zinc vacancies [42,43], and zinc interstitial [44]. Red luminescence was reported to be attributed to excess oxygen in samples, including oxygen interstitial defects, surface dislocations, and zinc interstitial [45-47].

In principle, the transition of electrons from the conduction band (CB) to holes in valence band (VB) emits a photon energy that can be detected by PL. This phenomenon is called intrinsic optical transition. Extrinsic transition results from impurities that introduce excess electrons or holes. For example, green luminescence (GL) represents impurities originating from defects that cause transition from the CB to a deep acceptor level because of zinc vacancies [45]. Figure 2.2 illustrates the transition of electrons from CB to VB in the presence of acceptor and donor in between, resulting in emissions of defects.

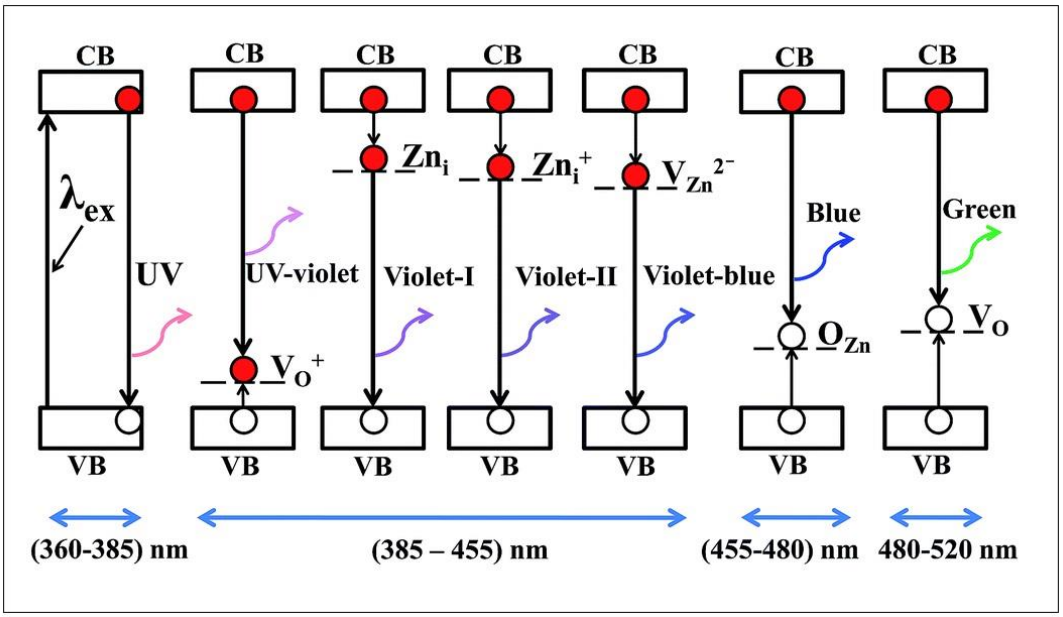

Figure 2.2: Illustration of electron transitions from the CB to VB and resulting luminescence in different wavelength ranges [42]

2.5.2 Raman scattering

Raman scattering in wurtzite structure of ZnO is measured using the source below the energy gap. This process will produce nonresonant Raman scattering [49]. In this study, we consider this type of scattering given that the laser source used was ionized argon laser at 514 cm^{-1}. The elementary unit cell of wurtzite crystal structure consists of four atoms, resulting in 12 phonon modes and nine that are optically active. According to group theory, at Γ-point of reciprocal space, optical phonon modes belong to the following [50]:

$$\Gamma^{opt} = 1A_1 + 2B_1 + 1E_1 + 2E_2, \qquad (2.1)$$

where A_1 and E_1 modes represent polars and can split into transverse optical (TO) and longitudinal optical (LO) phonons, respectively, and both are active in Raman and infrared (IR) spectroscopy. B_1 modes are IR and Raman inactive modes (silent modes). The two nonpolar low-frequency E_2 modes, E_2 (low), and high-frequency E_2 mode, E_2 (high), are Raman active only.

The first-order LO peak position in ZnO depends on crystallographic orientation of excited surfaces [51]. However, such orientation cannot be assumed to be caused by scattering of isotropic impurities. Excited surfaces may change propagation direction, neglecting the wave vector of phonons. Intensity and number of LO phonon lines observed in Raman spectra of ZnO-based materials also depend on grain size, impurities, defects, and free carrier concentration [52]. Cerquiera et al. (2011) [53] suggest that suppression of high-order LO phonon lines results from dissociation of excitons in ZnO. Alim et al. (2005) [54] reported redshift of LO phonon wavenumber in resonant Raman scattering. This shift was attributed to strong local heating by UV laser power. However,

nonresonant Raman scattering does not cause local heating. Thus, no redshift was observed. Redshift can occur in E_2 (high) mode in few cm^{-1} because of intrinsic defects [54].

2.5.3 Effects of annealing on morphology and optical properties of ZnO

ZnO properties can be altered by few treatments, such as doping, thermal annealing, and UV exposure [55]. Most treatments will affect optical, electrical, and morphological properties of ZnO depending on application. Many researchers have elaborated effects of annealing on ZnO, and numerous studies have been performed under several temperatures and conditions. Authors mainly highlight electrical, optical, and morphological properties of ZnO. Kumar et al. (2012) discussed effects of annealing on surface defects of ZnO after 200, 400, 600, and 800 °C [56]. Their results revealed increase in crystallinity with increase in temperature from 20 nm to 110 nm. Increase in annealing temperature also decreases visible emission with decreasing surface area to volume ratio. Annealing will also enhance UV emission and increase peak intensity. This condition is attributed to enhancement of ZnO crystal quality and decrease in defects after annealing.

Kushwala et al. (2013) discussed the effects of oxygen annealing on surface defects of ZnO nanowires [57]. Results revealed highly oriented ZnO nanowire after annealing in ambient oxygen condition. The authors plotted extremely strong orientation along the (002) plane and discovered that annealing improved crystal quality of nanowires. ZnO surface also absorbed oxygen chemically and reduced surface defects. Annealing changes concentration of oxygen vacancies at the surface and alters optical properties, which are investigated by PL spectroscopy [58]. Such changes include

suppression of defect band emission at GL and weakening of band edge emission at the UV region. These conditions are attributed to excess oxygen or creation of oxygen interstitial at the Zn surface. For Raman scattering, enhancement of E_2 (high) mode intensity at 439 cm^{-1} indicates improvement of oxygen content or reduction in oxygen vacancies in ZnO [59]. ZnO conductivity improves with increase in annealing temperature because of reduction in band bending at the ZnO surface and crystal quality improvement.

2.6 Bacterial structure

In general, bacteria are commonly found internally and externally of the human body. Each bacterium exhibits distinctive characteristics depending on its surroundings and functions. For example, bacteria on the skin, in oral cavity, and gastrointestinal tract will exhibit different functions and properties because of their different locations on the human body. Fig. 2.3 illustrates bacterial anatomy, and Table 2.1 simplifies functions of each part of the structure.

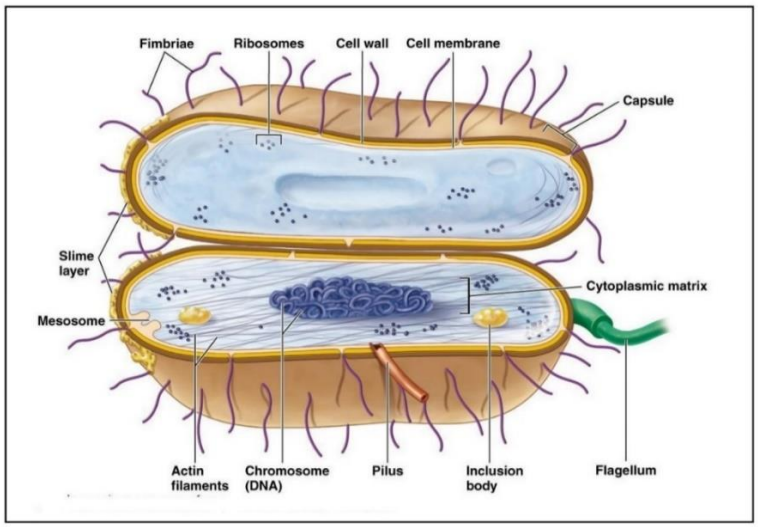

Figure 2.3: Structure of a typical bacterial cell [60]

Table 2.1: Function of the main components of a bacterial cell [60].

Components	Functions
Capsule or slim layer	Protects the cell and assist in attaching the cell to another surface
Cell wall	Protects the cell and gives shape to the cell
Cell membrane	Regulates movement of materials into and out of the cell: contains enzymes important in cellular respiration
Cytoplasm	Contains DNA, ribosomes and organic compounds required to carry out life processes
Plasmid	Contains some genes obtained through genetic recombination
Chromosome	Carries genetic information inherited from past generations
Pilus	Assist cell in attaching to other surfaces which is important for genetic recombination
Ribosomes	Ribosomes are the sites of proteins synthesis
Flagellum	Work as a tail that moves an entire cell

2.6.1 Oral *Streptococcus* bacterium

The human oral cavity is a complex and heterogeneous microbial habitat [61]. Saliva serves as good nutrient source and growth medium for bacteria in the oral cavity. In principle, oral bacteria are defined as microorganisms that live in the oropharynx and feature variable characteristics. Over 600 species of bacteria have been identified in the oral cavity, and they are predominantly aerotolerant anaerobes, such as streptococci and lactobacilli [61]. These bacteria can cause dental problems and periodontal diseases, such as dental plaque, dental caries, tooth decay, and gingivitis, because of improper oral hygiene [62].

In general, cell growth activities are divided into two ways or functions, namely, as biochemically catalytic (catalytic functions) and genetic coding activities (genetic functions). In catalytic functions, cells carry out metabolic chemical reactions. Genetic

functions replicate deoxyribonucleic acid (DNA), processing it to form ribonucleic acid (RNA) and proteins for maintenance and growth under prevailing conditions. Two main events are also observed in DNA processing, namely, RNA production (transcription) and protein production (translation), as illustrated in Fig. 2.4 [61].

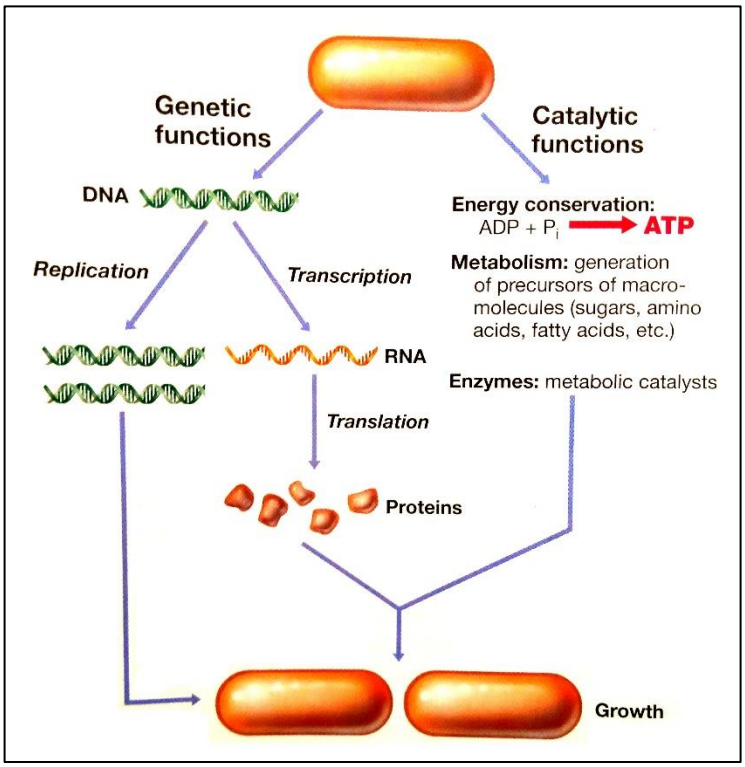

Figure 2.4: Illustration of replication, transcription, and translation during cell growth by catalytic and genetic functions [61]

2.6.2 *Streptococcus sobrinus* and *Streptococcus mutans*

This study places emphasis on bacteria implicated in dental caries. *S. sobrinus* and *S. mutans* [62] are bacteria involved in dental caries, and they are also classified as cariogenic bacteria. These oral streptococci are catalase-negative, Gram-positive cocci in chains and display spherical shape (cocci) with a diameter of approximately 0.5–0.8 µm.

In Gram-positive bacteria, the cell wall comprises 90% peptidoglycan. Peptidoglycan is a polysaccharide composed of two sugar derivatives and few amino acids, as illustrated in Fig. 2.5 [60,61]. Many Gram-positive bacteria possess several sheets of stacked peptidoglycan. As the peptidoglycan "matures," it forms a strong cell wall structure. Peptidoglycan can be destroyed by certain agents. Some important antibiotics, such as penicillin, target biosynthesis of peptidoglycan, eventually leading to osmotic lysis [61]. Gram-positive bacteria display a thick peptidoglycan cell wall layer at the cell wall structure compared with Gram-negative bacteria. This thick peptidoglycan comprises many layers. Wall-associated proteins, called teichoic acids, also stick out from this cell wall layer. Teichoic acids provide the negative charge which enables crystal violet to stick during washing (Gram staining).

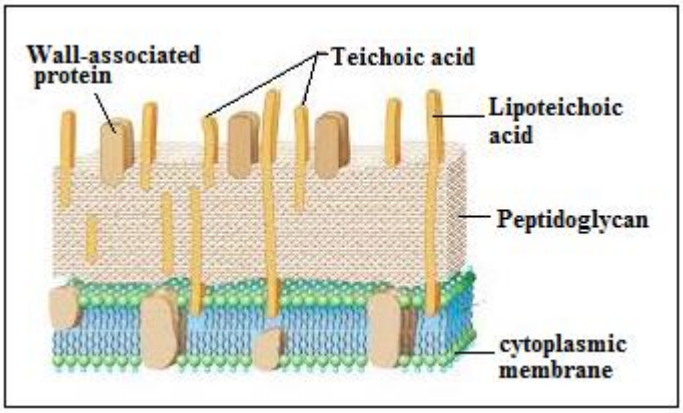

Figure 2.5: Schematic diagram of Gram-positive cell wall [61]

2.7 Antibacterial activity of ZnO

The ability of ZnO to inhibit growth of several types of bacteria has been reported [63-66]. At specific conditions, ZnO can kill certain bacterial species [67,68]. This antibacterial effect adds to the value of ZnO, which can be used in many products, such

as sunscreen [69], hospital wallpaper [70], personal care products [71], food packaging [72], and can be applied in leather color processing [63].

In principle, a number of mechanisms have been proposed to explain the potential antibacterial activity of ZnO. ROS generation from ZnO particles is discussed to influence bacteria in several ways [64,73]. These mechanisms include damaging and disorganizing the membrane cell wall through adhesion to the cell membrane [65,68], damaging membrane lipids [65], penetrating the cell membrane [74–76], and cellular internalization of particles [67].

ROS are formed by several ways during the interaction of bacteria and ZnO particles. Fig. 2.6 shows ROS types, such as superoxide anions, hydroxyl radicals, hydroxyl ions, and hydrogen peroxide [77].

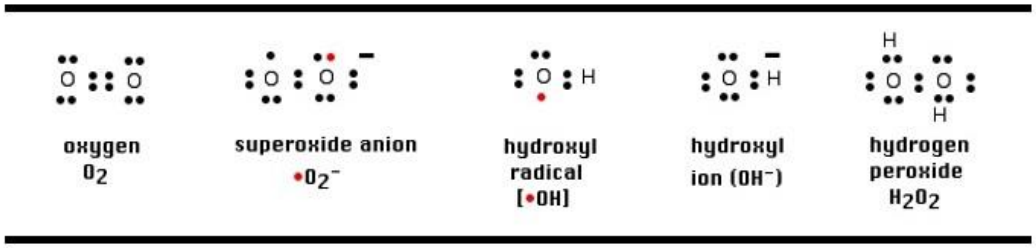

Figure 2.6: Types of ROS. Red marks indicate unpaired electrons

ROS generation relies on existing electron–hole pair in ZnO surface. The hole in VB will react with water molecules (H_2O) or hydroxide ions adsorbed on the surface to produce hydroxyl radicals (·OH). Subsequently, the electron in CB will reduce O_2 to produce superoxide ions ($\cdot O_2^-$). When contacting with organic compounds, both hole and ·OH become extremely reactive. Other ROS, such as hydrogen peroxide (H_2O_2), can also be detected.

2.8 Minimum Inhibition Concentration (MIC) and Minimum Bactricidal Concentration (MBC)

In antimicrobial activity, MIC is defined as the smallest amount of material needed to inhibit growth of microorganism. MBC represents the minimum amount of material that kills microorganisms. In antimicrobial susceptibility testing, two types of testing, namely, broth dilution and disk diffusion technique, are used to determine MIC and MBC for selected microorganisms. According to CLSI M11-A8 [78], broth dilution technique is a user-friendly method and appropriate for new materials. Therefore, in this method, MIC is determined at growth start to inhibit cut point of less turbidity, whereas MBC is measured when no viable colony occurred after 24 h incubation, as depicted in Fig. 2.7.

Yousef (2012) reported the same value for both MIC and MBC of nano ZnO [79]. However, different microorganisms may feature different levels of sensitivity or resistance toward the same type of ZnO particle, thus yielding different MIC and MBC values [80-82]. For example, Singh (2013) reported MICs for *Escherichia coli* (Microbial Type Culture Collection and Gene Bank (MTCC 443), *Staphylococcus aureus* (MTCC 3160), and *Bacillus subtilis* toward the same ZnO particle at 12.5, 12.5, and 25 µg/ml, respectively [81]. Sevinç (2010) [82] reported 50 µg/ml MIC and 150 µg/ml MBC for commercially uncoated ZnO on *S. sobrinus* (American Type Culture Collection (ATCC) 27352). Discrepancies may be influenced by preparation method, particle size, targeted strain, different types of cell membrane (Gram-positive or Gram-negative), presence of catalase, shapes, and serotype. Therefore, using microorganisms that have been recognized and purely isolated from established companies, such as ATCC or

MTCC, is recommended. This method may help prevent microorganism heterogeneity, wherein two or more types of bacterial strains grow in one colony.

Recently, studies have reported less information about MIC and MBC of ZnO structure on cariogenic microorganisms. Therefore, this study focuses on MIC and MBC determinations to address safety issues for ZnO application as temporary dental restorative material.

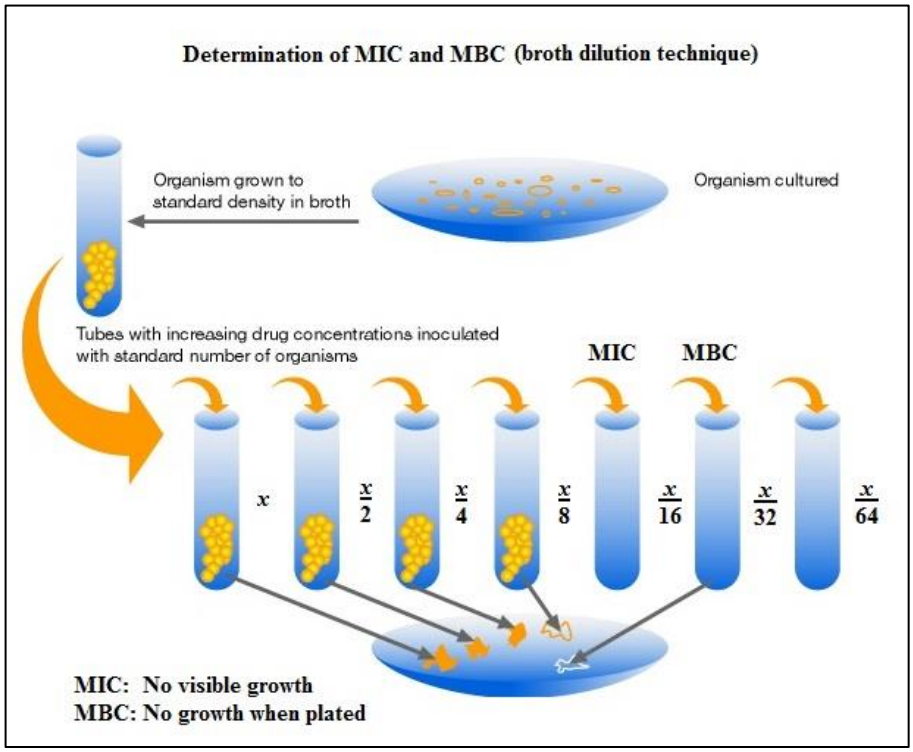

Figure 2.7: Illustration of MIC and MBC determination by broth dilution technique [83]